Twelfth Australasian Fluid Mechanics Conference
The University of Sydney, Australia 1995

SPATIAL AND TEMPORAL CHARACTERISTICS OF BOUNDARY LAYERS CONTROLLED WITH THE LORENTZ FORCE

Daniel M. Nosenchuck, Garry L. Brown, Harry C. Culver, Thomas I. Eng and Irene S. Huang

Department of Mechanical and Aerospace Engineering
Princeton University
Princeton, New Jersey
USA

ABSTRACT

Experiments aimed at restructuring laminar and turbulent boundary layers, primarily for the purpose of skin-friction reduction, were performed on a flat-plate in a water tunnel filled with a mild solution of NaOH. Arrays of flush-mounted electrodes and sub-surface magnets were used to induce a current-density field **j**, and magnetic field **B**, in the vicinity of the wall to provide a three-dimensional body-force $\mathbf{j} \times \mathbf{B}$ (the Lorentz force). The curl of this Lorentz force represents a vorticity source-field that directly interacts with, and redistributes, the boundary-layer vorticity. Tiles are enabled in spatially- and temporally-periodic patterns to induce global modification of the near-wall flow characteristics. Vorticity waves were observed to form in laminar boundary layers at a 'resonant' operating point. Corresponding wall-shear reductions up to 90% were measured. A similar response was noted in turbulent boundary layers over less narrowly-tuned operating points with substantial (>50%) decreases in viscous skin-friction.

BACKGROUND

In our initial experiments, the concept of creating a steady Lorentz force in a boundary layer, for the purpose of turbulent wall-shear control, was demonstrated in a flow with non-uniform electrical conductivity (Nosenchuck and Brown, 1993). The Lorentz force-field acted principally perpendicular to the wall and suppressed the turbulent motions near the wall leading to substantial reductions in Reynolds stress and the wall shear. The idea in the present experiments was to examine the effect of imposing on the fluid in a turbulent-boundary layer an *unsteady* Lorentz force ($\mathbf{j} \times \mathbf{B}$) in a *uniform* electrolyte using an array of tiles oriented such that the only mean spatial component of the force field was *perpendicular* to the wall.

A distinguishing feature of the Lorentz-force actuator (LFA) was that it imparted a direct volumetric body-force control to the fluid. This was a marked departure from typical two-dimensional actuators, (e.g. surface motion, blowing/suction, heating/cooling) which often rely on indirect means to affect the bulk flow.

The present approach is in contrast to 'traditional' electromagnetic flow control which has generally been accomplished either using magnetohydrodynamic (MHD) principles that typically relied on large, steady, magnetically-induced fields ($\mathbf{u} \times \mathbf{B}$) in highly conducting fluids to provide direct damping of all turbulent fluctuations (Ferraro 1966, Fraim and Heiser 1968), or used streamwise components of MHD forces (Rossow 1958, Watanabe 1978) to provide a thrust or drag.

LORENTZ-FORCE ACTUATORS

A single tile, called a Lorentz-force actuator (LFA) is shown in Figures 1a and 1b. The spatially-averaged

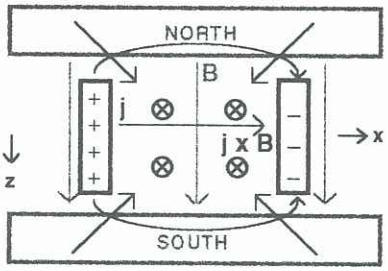

FIGURE 1A: LFA TILE PLANFORM VIEW

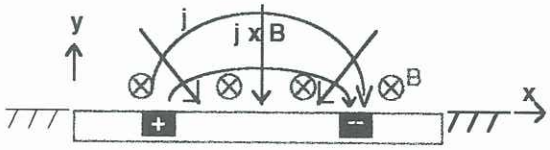

FIGURE 1B: LFA TILE ELEVATION VIEW

Lorentz force provides a net wall-normal force, with no components parallel to the surface, due to the symmetry of the LFA. Local normal components of both the **j** and **B** fields give rise to wall-parallel forces which have mirror symmetry about the longitudinal and lateral axes that pass through the center of the tile. In the illustration above, the magnet-axes are streamwise; similar behavior results for other orientations, such as spanwise (see Figure 4b below).

Gradients in the Lorentz force generate a three-dimensional vorticity source in the fluid. This is readily observed by including the Lorentz force in the momentum equation, and then taking the curl, to obtain

$$\rho \frac{D\boldsymbol{\omega}}{Dt} = \rho(\boldsymbol{\omega} \cdot \nabla)\mathbf{u} + \mathbf{Q}_{\omega}, \qquad (1.)$$

where $\mathbf{Q}_{\omega} \equiv \nabla \times (\mathbf{j} \times \mathbf{B})$ represents a source of vorticity. Thus, the LFA provides the capability to introduce spatially- and temporally-controlled vorticity for the purpose of globally restructuring the boundary layer. To illustrate this LFA characteristic, the two-dimensional form of Equation (1) is written in a 'characteristic' form

$$\rho \frac{D\boldsymbol{\omega}}{Dt} = \mathbf{Q}_{\omega} \qquad (2.)$$

A simple graphical solution may be obtained for the case where the velocity perturbation is small, so that the characteristic slope $dx/dt \approx U_c(y)$, where U_c is the convective speed at a particular height y above the surface. Based on the geometry of the tile the source $\mathbf{Q}_\omega$ is anti-symmetric about x = 0. This may be crudely approximated by a series of Heaviside functions to provide $\pm \mathbf{Q}_0$ at height y. Figure 2 shows a graphical solution to Equation 2 for such a source. Two active tiles are separated by one inactive tile in the streamwise direction. Both tiles are activated as indicated on the temporal ordinate. As depicted in the

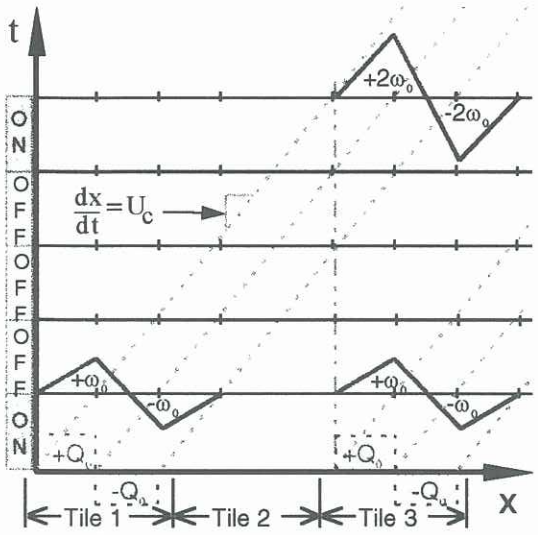

FIGURE 2: RESONANT VORTICITY GENERATION AT A HEIGHT Y

Figure, fluid elements acquire vorticity by integrating $\mathbf{Q}_\omega$ as they advect over the tiles. The activation frequency is chosen to reinforce the vorticity input by upstream tiles. This condition is called *resonance*. The duty cycle is chosen to provide peak positive and negative regions of vorticity.

Figure 3 shows a typical plot of the source of spanwise vorticity, $\mathbf{Q}_{\omega(z)}(x,y)$, over the centerline of a single LFA

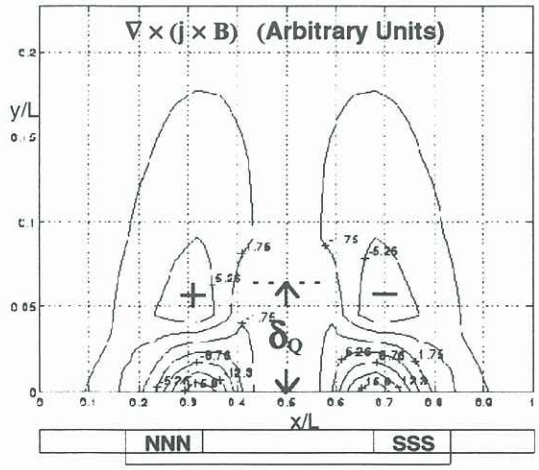

FIGURE 3: ANSYS SOLUTION OF ∇× (j × B)

tile, and oriented such that the longitudinal magnet axis is 90° to the x-direction. It is based on an ANSYS finite-element simulation of the current-density and magnetic fields. As is evident in this Figure, the source is anti-symmetric about x = 0, and has a local maximum away from the wall at δ_ω. Fluid elements acquire vorticity as they move through this source-field. (It is noted that since the circulation on a flat plate per unit length is U_∞, and remains unchanged by the LFA, the total spanwise (and streamwise) vorticity induced by the LFA is zero.)

EXPERIMENTAL SETUP

Experiments were performed to determine the effect such a vorticity source-field has on the boundary layer, particularly on the skin-friction. To cover an arbitrarily large area and maintain significant **j** and **B** field-strength near the wall, an array of LFA tiles was used as shown in Figure 4. The particular geometry of the tile (e.g. magnet and electrode dimensions and spacings) is designed to create an appropriate vorticity source above

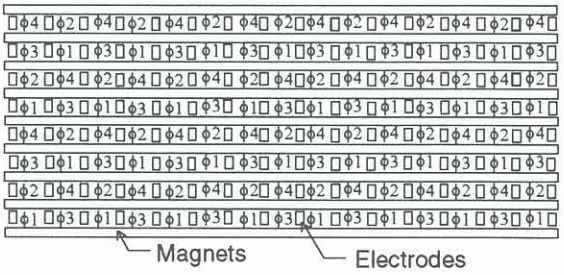

FIGURE 4A: 8 × 15 LONGITUDINAL LFA ARRAY

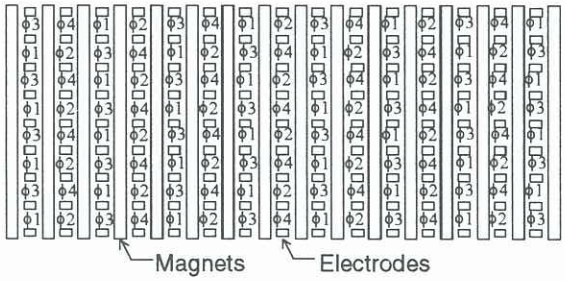

FIGURE 4B: 8 × 15 LATERAL LFA ARRAY

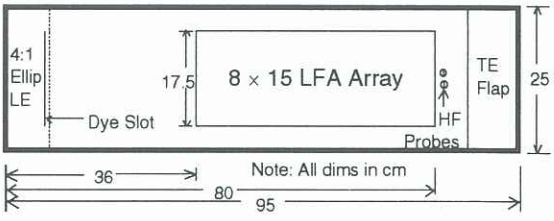

FIGURE 4C: FLAT-PLATE MODEL LAYOUT

the tile. Two array configurations were examined: one with longitudinal magnets (Figure 4a) and one with lateral magnets (Figure 4b). In both cases, the flow over the array is from left to right.

Streamwise-adjacent tiles share a common electrode, and thus cannot be simultaneously energized. Spanwise-adjacent tiles share a common magnet where the local magnetic field is normal to the pole. Thus, to prevent stray Lorentz forces, spanwise-adjacent tiles are not simultaneously energized. Therefore, as shown by

the phase distribution (ϕ) in Figures 4a,b, a maximum of one-quarter of the tiles are energized at any given time, with a maximum duty cycle of 25%. In the present experiments it was desired to promote a vorticity source field that strengthened with increasing downstream distance, and study its interaction with the mean boundary-layer vorticity, $\overline{\omega}_z$. Thus, a series of resonantly-reinforced traveling waves were created. For the case of the streamwise magnet-array (Figure 4a), a spatially oblique vorticity source was created with a simple four-phase pattern:

$$\phi_1 \rightarrow \phi_2 \rightarrow \phi_3 \rightarrow \phi_4 \rightarrow \phi_1 \rightarrow \phi_2 \rightarrow \phi_3 \rightarrow \phi_4 \rightarrow \ldots .$$

A two-dimensional vorticity wave was generated by operating the array (Figure 4b) with a phasing pattern that had a long dwell time in alternate rows, i.e.:

$$\phi_1 \rightarrow \phi_3 \rightarrow \phi_1 \rightarrow \phi_3 \rightarrow \phi_1 \rightarrow \phi_3 \rightarrow \phi_1 \rightarrow \phi_3 \rightarrow$$
$$\phi_2 \rightarrow \phi_4 \rightarrow \phi_2 \rightarrow \phi_4 \rightarrow \phi_2 \rightarrow \phi_4 \rightarrow \phi_2 \rightarrow \phi_4$$

which then repeats. This 16-phase pattern generates phase fronts which are planar within 1/16 of the streamwise wavelength. Both array configurations and phasing patterns produced qualitatively similar results. The particular arrays used to produce the present results had eight spanwise and 15 streamwise tiles, and was fabricated with permanent rare-earth NIB (neodymium-iron-boron) magnets ($|\mathbf{B}|_{max}$ = 0.35 T) and stainless-steel electrodes. The characteristic tile size was arbitrarily chosen to scale with a nominal laminar boundary layer thickness, $\delta_{0.99}$, at the trailing edge of the tile-array at $Re_x = O(10^5)$. The location of the array in the flat-plate model is shown in the layout diagram in Figure 4c.

FLOW VISUALIZATION

Experiments were performed in a water tunnel filled with a mild aqueous NaOH solution (σ = 2.5S/m). The primary diagnostics were flush-mount hot-film probes and laser-induced flow-visualization (LIF). Disodium fluorescein was injected into the boundary layer through a spanwise slot in a 4:1 elliptical leading edge. In the case of the streamwise-magnet array (Figure 4a), the laser-sheet was initially positioned in the vertical streamwise (x,y) plane and centered over magnets near the trailing-edge of the array. At U_∞ = 7.5 cm/s, with a peak electrode voltage of 4.5V and 0.7A total current, resonantly-reinforced traveling waves emerged at a frequency f = $0.6(U_\infty/d)$ as visualized with LIF in Figure 5. Rotational structures are evident in the outer portion of the boundary (Figure 5a). When the laser sheet was re-positioned at the tile centerline (Figure 5b), similar rotational structures were visible, but appear to lie farther from the wall. The uncontrolled boundary layer is seen to be substantially thinner (Figure 5c). Quantitative measurements later indicated that the thicker controlled boundary layer corresponds to a relatively lower wall-shear.

A spanwise laser sheet (y-z plane) was introduced through the tile centers in the third row from the downstream edge of the LIF array. As shown in Figure 6, a counter-rotating structure is visible in the laser sheet, and apparently has a rotation axis with longitudinal components. This departure from a purely two-dimensional rotational wave is most likely due both to spanwise variability in $\mathbf{Q}_{\omega(z)}$ and the presence of a longitudinal vorticity source $\mathbf{Q}_{\omega(x)}$.

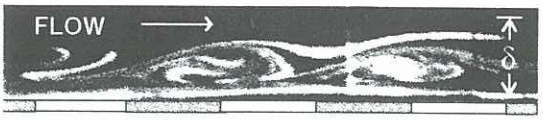

FIGURE 5A: LFA ARRAY ON: TILE-EDGE LIF

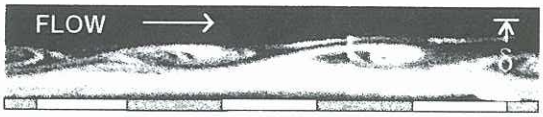

FIGURE 5B: LFA ARRAY ON: TILE-CENTER LIF

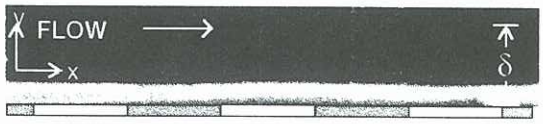

FIGURE 5C: LFA ARRAY OFF

FIGURE 6: SPANWISE (Y-Z) LIF

QUANTITATIVE CHARACTERISTICS

Velocity and Vorticity

Velocity profiles, u(y), were obtained with a hot-film traverse of a Blasius boundary layer at the tile center-point adjacent to the trailing-edge and centerline of the LFA array for the four-phase forcing pattern at 4.0Hz phasing frequency and 2.5V peak electrode voltage. Three-periods of phase-locked ensemble-averaged velocity perturbations are presented in Figure 7a. Strong wave-like behavior is observed near $y/\delta \approx 0.2$ with approximately a 180° phase shift across the layer.

The velocity data were differenced in the normal direction to determine $-\partial u/\partial y$. This quantity was approximately representative of the boundary-layer vorticity. The behavior of the 'vorticity' under LFA control (four-phase forcing) is shown in Figure 7b as a time-series (solid lines) corresponding to 30° intervals of a single period. Relative to the Blasius vorticity distribution (dashed lines), the average vorticity at the wall has *decreased*. Since the LFAs introduce no net circulation in the boundary layer, the 'total vorticity' is unchanged. Thus, the likely action of the LFAs is to redistribute the vorticity to an *increased height*. This is seen as an increase in the 'vorticity' at $y/\delta \approx 0.4$.

Wall Shear-Stress

To determine the effect of the LFA array on skin-friction, two spanwise flush-mount hot-films were mounted one tile spacing, d, downstream of the trailing edge of the array as shown in Figure 4c. Typical time series of normalized skin-friction (corresponding to early transitional flow) at the tile center and edge are shown in Figure 8. The LFA array produces a substantial reduction in the wall stress with an average value in excess of 50% (peak reduction at the centerline near 90%). The spanwise variation in stress is likely related to the spanwise and streamwise variations in

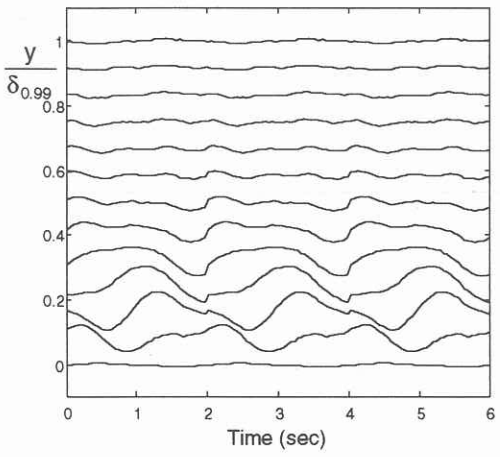

FIGURE 7A: VELOCITY PERTURBATION TIME-SERIES AT TILE CENTER

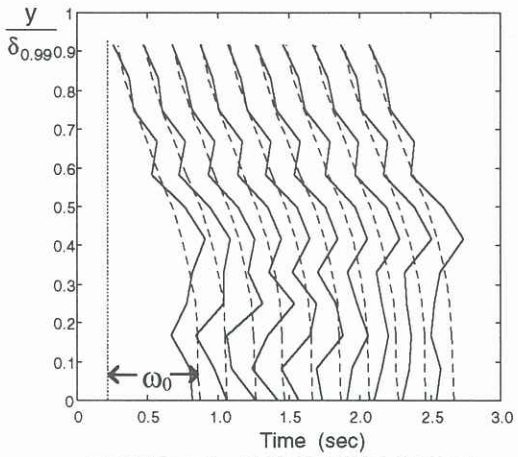

FIGURE 7B: -DU/DY TIME-SERIES
U_∞ = 0.075 m/s, Re_x = 6.1×10⁴

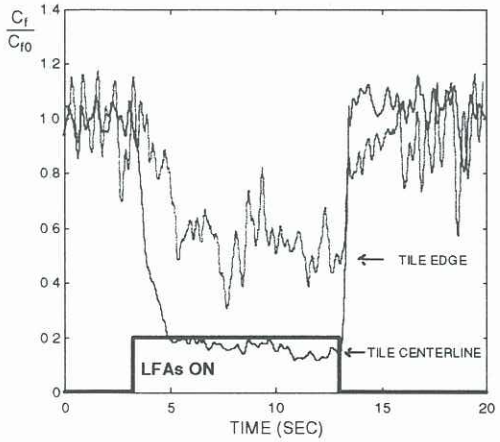

FIGURE 8: WALL SHEAR TIME-SERIES
U_∞ = 0.525 m/s, Re_x = 4.2×10⁵

the vorticity introduced by the tiles, as noted above.

LFA control of turbulent boundary-layer wall-shear is shown in Figure 9 for $5\times10^5 \le Re_x \le 3.6\times10^5$. Viscous stress reductions increase with Re (velocity) to ~55%. It may be speculated that the decrease in the boundary-

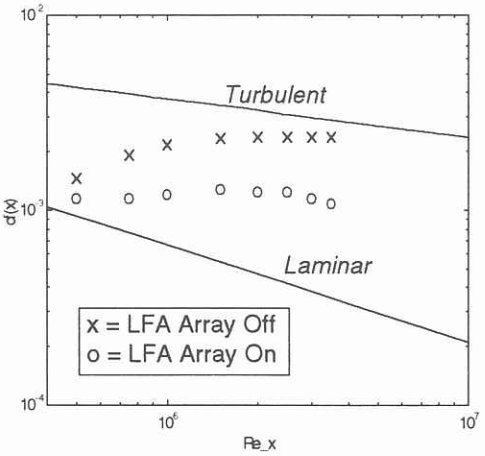

FIGURE 9: TURBULENT DRAG REDUCTION

layer vorticity scale-height provided a stronger coupling with $\mathbf{Q}_\omega$ whose scale height is δ_Q (see Figure 3).

CONCLUSION

An hypothesis for the observed effects is that the curl of the Lorentz force is a source of vorticity which through an interaction with the near-wall vorticity leads to a direct restructuring of the vorticity field in a laminar boundary layer, and affects the coherent motions responsible for turbulence production in high-Re boundary-layers.

ACKNOWLEDGMENTS

The authors thank Mr. Thomas Frobose for his skill, help, and patience, and appreciate the early support of NSF Grant CTS9223119. The contractual support and partnership of Nova Innovations Inc. and McDonnell Douglas Technologies Inc., and their help with many of the key technologies which was critical for this work is gratefully acknowledged.

REFERENCES

Ferraro, V.C.A., and Plumpton, C., 1966 "An Introduction to Magneto-Fluid Mechanics," Clarendon Press, Oxford, 2nd ed., p.150.

Fraim, F.W., and Heiser, W.H., 1968 " The Effect of a Strong Longitudinal Magnetic Field on the Flow of Mercury in a Circular Tube," *Journal of Fluid Mechanics*, Vol. 33, pp.397-413.

Nosenchuck, D.M., and Brown, G.L., 1993, "The Direct Control of Wall Shear-Stress in a Turbulent Boundary Layer," *Proceedings of the International Conference on Near-Wall Turbulent Flows*," Elsevier, pp.689-698.

Rossow, V.J., 1958, "On Flow Of Electrically Conducting Fluid Over A Flat Plate In The Presence Of A Transverse Magnetic Field," NACA TR 1358 (1958).

Watanabe, T., 1978, "MHD Stability of Boundary Layers Along a Flat Plate in the Presence of a Transverse Magnetic Field," ZAMM, Vol. 58, p.555.